

VENTED EXPLOSION OVERPRESSURES FROM COMBUSTION OF HYDROGEN AND HYDROCARBON MIXTURES

Bauwens, C.R., Chaffee, J. and Dorofeev, S.B.

FM Global, Research Division, 1151 Boston-Providence Turnpike, Norwood, 02061, USA,
sergey.dorofeev@fmglobal.com

ABSTRACT

Experimental data obtained for hydrogen mixtures in a room-size enclosure are presented and compared with data for propane and methane mixtures. This set of data was also used to develop a three-dimensional gasdynamic model for the simulation of gaseous combustion in vented enclosures. The experiments were performed in FM Global's 64 m³ chamber, a 4.6 x 4.6 x 3.0 m chamber with a vent opening on one side. Vent areas of either 2.7 or 5.4 m² were used. Tests were performed with ignition either at the center of the chamber or at the center of the wall opposite the vent. Hydrogen-air mixtures with hydrogen concentrations close 18% vol., stoichiometric propane-air and stoichiometric methane-air mixtures were used in these tests. Pressure data, as function of time, and flame time-of-arrival data were obtained both inside and outside the chamber near the vent. Modeling was based on a Large Eddy Simulation (LES) solver created using the OpenFOAM CFD toolbox using sub-grid turbulence and flame wrinkling models. A comparison of these simulations with experimental data is discussed.

NOMENCLATURE

a	model parameter	Greek	
b	combustion regress variable	δ	flame thickness (m)
Le	Lewis number	Ξ	flame surface wrinkling factor
L_T	integral turbulent length scale (m)	λ	wavelength
n	wave number	Δ	filter size
Pe	Peclet number	σ	expansion ratio
r	flame radius	subscripts	
u'	turbulent intensity (m/s)	T	turbulent
S_L	laminar burning velocity (m/s)	I	instability
t	time (s)	c	cut-off
		cl	critical
		m	maximum

1.0 INTRODUCTION

Explosion venting can be used to prevent or minimize damage to an enclosure by relieving the pressure within the volume and is an important engineering loss prevention solution. Experimentally, the subject of vented explosions has been widely studied with research performed over a range of scales, from laboratory scale tests (see, e.g., [1]) to large scale tests (see e.g., [2, 3, 4]). Factors contributing to the pressure build-up in vented explosions have been extensively studied [1, 2, 3, 4, 5, 6, 7, 8].

Analytical models and empirical correlations have also been developed (see, e.g., [8, 9, 10, 11]), a number of which have been included in engineering guidelines [12, 13]. These correlations however, often have conflicting recommendations. This is due to the complex nature of the process itself, as mentioned above, and the influence of other factors that can affect the peak overpressure, such as size

and shape of the enclosure, the mixture being burned, the type of vent and vent deployment pressure, congestion or obstacles inside the chamber and the ignition location.

Computational Fluid Dynamics (CFD) simulations of vented explosions, and the comparison of these simulations with experimental data [4, 14, 15], have shown some of the challenges involved in adequately modeling the major physical phenomena involved. Although there are a few examples of successful CFD applications for several selected tests, such as [15], it is not unusual to find CFD predictions that are off the test results by more than an order of magnitude.

Because of the limited reliability of the current methods for the prediction of pressure generation during a vented explosion, a research project was initiated at FM Global with the goals of generating a set of experimental data as well as developing and validating a computational code and new engineering tools. The first part was performed for low reactivity stoichiometric methane-air mixtures [16]. The lean hydrogen mixtures used in the present study however, present additional challenges. This is mainly due to two factors. First, that the hydrodynamic flame instability is enhanced by thermal diffusion effects, which results in a significant increase in the flame surface for lean hydrogen mixtures. And the second is the effect of the Lewis number on the turbulent burning velocity. Currently, the strength of these effects is not known well enough to be reliably modeled. Comparisons with stoichiometric methane-air and propane-air mixtures illustrate the significant differences caused by these instabilities and yield some insight on how to model them.

The objectives of the present work are to (i) examine the similarities and differences between three mixtures of similar laminar flame speed, 18% hydrogen-air, 9.5% methane-air and 4.0% propane-air; (ii) test an extension to the numerical CFD model developed in the previous study and identify its capabilities and deficiencies to describe the physics responsible for the pressure build-up.

2.0 EXPERIMENTS

The data presented here were obtained from experiments performed at the FM Global 64 m³ large scale explosion test chamber. The overall dimensions of the test chamber were 4.6 x 3.0 x 4.6 m with a square vent of either 5.4 m², or 2.7 m² located on one of the vertical walls. Four chamber pressure transducers were mounted to the chamber, one at the center of the wall opposite the vent, one on the wall containing the vent, and two on a wall perpendicular to the vent (one on-axis with the center of the chamber, one off-axis), (see Fig. 1 below). The geometry is also illustrated by Fig. 2 below. Twenty flame time-of-arrival thermocouples, at a height of 1.4 m above the floor of the chamber, were placed at 0.5 m intervals inside the chamber along two axes and at 1 m intervals outside of the chamber. Two blast-wave pressure transducers were installed in a concrete slab outside of the chamber, below the line of thermocouples at a height of 0.3 m above the ground, 1.17 m and 3.45 m from the vent. One high speed and four low speed cameras were used to observe the tests, either directed into the chamber or directed outside to capture the external explosion. Data was collected using a 32 channel high speed data acquisition system sampling at a rate of 25,000 scans/sec.

The initial mixture was supplied by injecting the pure fuel through an inlet at the floor of the chamber while mixing fans within the chamber were used to create a uniform mixture. The concentration of gas inside the chamber was controlled using a Cirrus mass spectrometer. The unburned mixture was contained within the chamber (prior to ignition) using a 0.02 mm thin sheet of polypropylene. Ignition was supplied using a carbon rod igniter at one of two locations, either I₁, the center of the chamber or I₂, 0.25 m from the center of the wall opposite the vent, also referred to as back-wall ignition. The time between when the mixing fans were stopped and ignition was controlled to ensure a consistent initial turbulent intensity ($u' \approx 0.1$ m/s), which was determined in a series of preliminary tests using measurements from a bi-directional velocity probe.

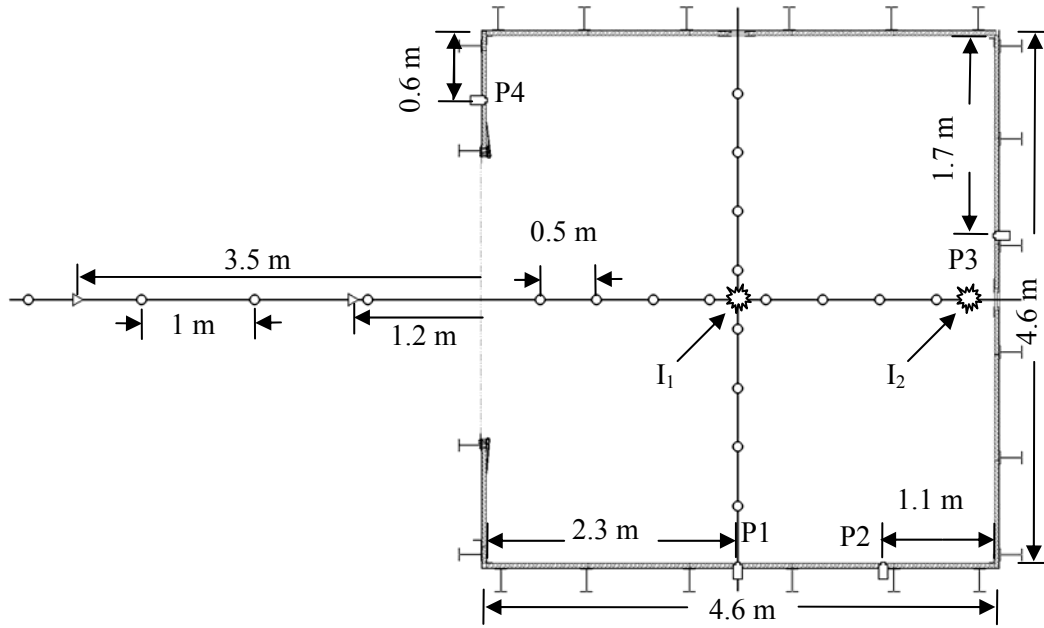


Figure 1. Illustration showing the locations of pressure transducers, (rectangles), flame arrival thermocouples (circles), blast-wave pressure transducers (triangles) and ignition locations I_1 (center) and I_2 (back-wall).

In this study three mixture compositions were examined: 18% vol. hydrogen-air, 9.5% methane-air and 4.0% propane-air. For these three mixtures experiments were performed for two ignition locations, center and back-wall, and with two vent sizes 2.7 m^2 and 5.4 m^2 . A total of 24 tests for these configurations were performed, including tests for repeatability.

3.0 NUMERICAL SIMULATIONS

3.1 Solver Details

The numerical simulations were performed using a custom solver built using the OpenFOAM CFD toolbox [17]. The code is based on a Large Eddy Simulation (LES) solver of the Navier-Stokes conservation equations for mass, momentum and energy using a robust, implicit, pressure-velocity, iterative solution framework, with a fully compressible Pressure-Implicit Split Operator (PISO) solution method [18]. The sub-grid scale turbulence model used was a one-equation eddy viscosity model [19].

An unstructured grid was used for the current study. Second order schemes were used in space and time, central differencing for velocity, a bounded TVD scheme for scalars, and a second order backward differencing scheme for time.

The combustion model is based on a transport equation for a regress combustion variable b [20]. The transport of the regress variable is governed by a laminar burning velocity, S_L and a flame surface wrinkling factor, Ξ . The scalar flame surface wrinkling factor, Ξ , was transported to take into account the effect of flame wrinkling on the burning velocity.

Flame instabilities in a lean hydrogen-air mixture can produce a significant increase in the flame's surface area and propagation speed. This effect was incorporated into the model using Eq. (1) below,

$$\Xi = \Xi_I \Xi_T, \quad (1)$$

where Ξ_I is the surface wrinkling factor due to hydrodynamic flame instabilities and Ξ_T is the surface wrinkling factor due to turbulence. The form of Eq. (1) suggests that the characteristic length scales of the two types of wrinkling are different.

The Ξ_I term in Eq. 1 may be expressed as [21]:

$$\Xi_I = \left(\frac{\lambda_m}{\lambda_c} \right)^{1/3}, \quad (2)$$

where λ_m is the maximum unstable scale and λ_c is the cutoff wavelength. In a sub-grid model $\lambda_m \leq \Delta$, where Δ is the filter size. Experimentally, the onset of instability is observed for sufficiently large Peclet numbers, $Pe = r/\delta > Pe_{cl}$, where r is the flame radius, and Pe_{cl} is the critical Pe number [22, 23]. The cutoff scale is given by:

$$\lambda_c / \delta = 2\pi Pe_{cl} / n_{cl}, \quad (3)$$

where n_{cl} is the critical wave number and is of the order of 10. This yields the following equation for Ξ_I :

$$\Xi_I = \max \left[1, a_I \left(\frac{\Delta}{\lambda_c} \right)^{1/3} \right] \quad (4)$$

where a_I is a coefficient to account for the uncertainty in λ_c . In cases when $a_I(\Delta/\lambda_c)^{1/3} < 1$, flame instabilities are expected to be resolved on the grid scale and $\Xi_I = 1$. This was the case in [16] where methane-air mixtures were used. For an 18% hydrogen-air mixture at 365K the cutoff scale is estimated as $\lambda_c = 7$ mm [23]. The value of λ_c for normal initial temperature is unknown. In the current study the values of $\lambda_c = 7$ mm and $a_I = 1.2$ were used to get agreement with the initial flame propagation velocity.

The surface wrinkling factor due to turbulence, Ξ_T was computed using a transport equation taking into account the generation and removal of flame surface wrinkling. The equilibrium Ξ_T , Ξ_{eq}^* is given by the following turbulent burning velocity correlation [24]:

$$\Xi_{eq}^* = 1.48 \cdot (u' / S_L)^{1/2} (L_T / \delta)^{1/6} a_T Le^{-n}, \quad (5)$$

where u' is the turbulent intensity, L_T is the integral turbulent length scale, Le is the Lewis number, and a_T is a constant. The factor a_T is used because the value of the burning velocity predicted by Bradley's correlation is only estimated within a factor of 2. Also, the turbulent burning velocity is known to increase as Le decreases. Bradley et al. [24] suggested $n = 0.3$, while Driscoll [25] derived $n = 1$ based on the same data. A value of $a_T Le^{-n} = 0.7$ was used for all simulations, which provided good agreement for flame speeds with the experimental results.

3.2 Mesh Geometry, Initial and Boundary Conditions

An unstructured computational mesh was generated for the 64 m³ explosion test chamber geometry matching the major significant features of the experimental setup (Fig. 2). An external volume of 25.0 x 20.0 x 16 m was also meshed to capture the venting of burned gas, the external explosions and to reduce the effect of non-ideal boundary conditions. A cell size of 5 cm was used in the region inside the chamber and the area immediately outside the chamber to resolve the external explosion. This

yielded a computational mesh of approximately 10^6 cells, the limit for a reasonable study. Finer and coarser meshes with cell sizes of 3 cm and 7.5 cm inside the chamber were also tested. Flame speeds and maximum overpressures appeared to be within $\pm 8\%$ for all of the meshes, and grid convergence was found to be acceptable.

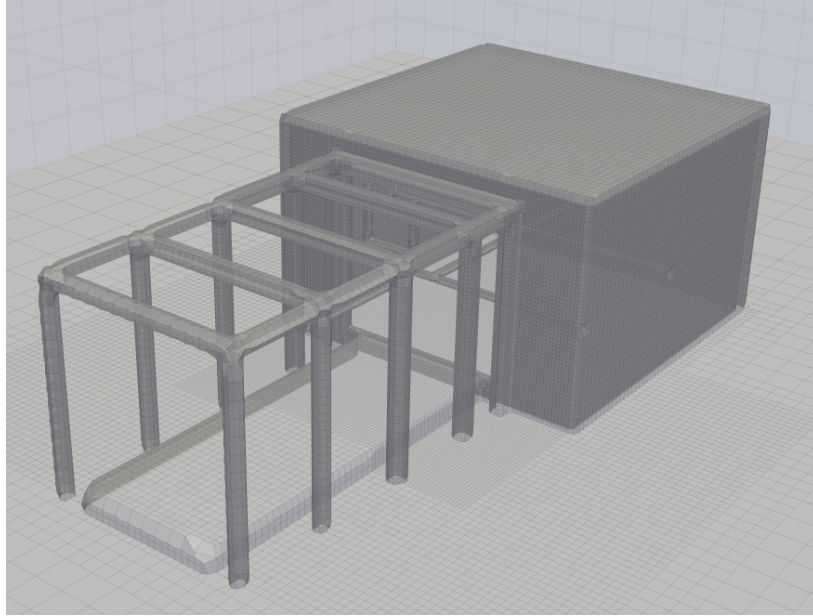


Figure 2. The geometry of the computational domain used in the numerical simulations.

The boundary conditions applied to the geometry were non-slip adiabatic walls for the chamber walls and ground, and wave transmissive pressure boundary conditions were used for the free boundaries to minimize reflections. An unrestricted open vent was used in the simulations. The initial level of turbulence $u' \approx 0.1$ m/s was imposed to match the initial conditions observed in the experiments.

4.0 RESULTS

4.1 Experimental Results

A filtered and unfiltered pressure time history of a 17.7% hydrogen-air mixture with center ignition and a 5.4 m² vent is shown below in Fig. 3 as an example of a typical pressure time-history for a vented explosion of a hydrogen mixture. An 80 Hz low pass filter was used to remove the higher frequency component of the pressure signal and isolate the overpressures acting at a sufficiently low frequency to present potentially damaging pressure loads.

Multiple pressure peaks and high-frequency oscillations are clearly visible in Fig. 3. These peaks originate from the interactions between various effects such as Helmholtz oscillations and the external explosion that can result in the Taylor instabilities that have been previously observed [1, 16]. It can also be seen that, immediately following the first peak related to the external explosion, high frequency acoustics centered about 700 Hz with a range of ± 100 Hz, corresponding to the natural frequencies of major structural components of the chamber, are also excited.

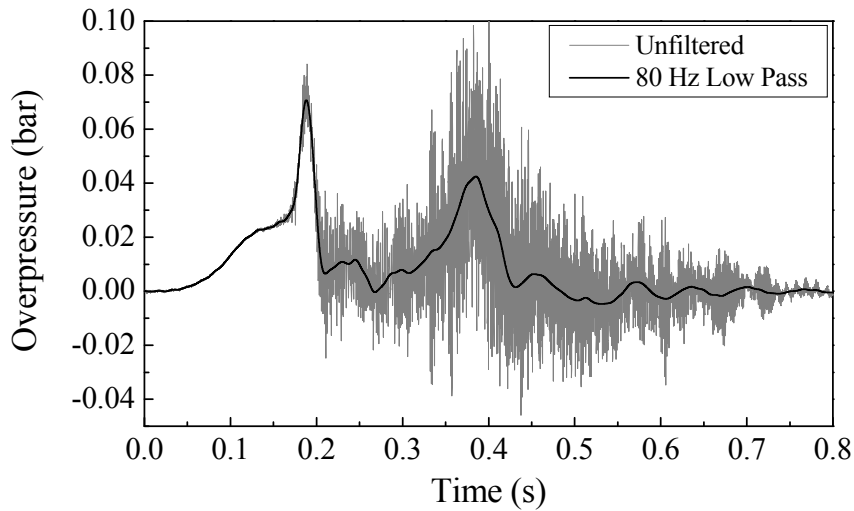


Figure 3. Filtered and unfiltered pressure time history for a 17.7% hydrogen-air mixture ignited with central ignition and a 5.4 m² vent

4.2 Effect of Mixture Composition

Table 1. Summary of flame speed parameters for mixtures studied.

Mixture	Laminar Burning Velocity, S_L (m/s)	Expansion Ratio, σ	Flame Speed, $(\sigma \times S_L)$ (m/s)	Average Measured Initial Flame Speed, U_0 (m/s)
4.0% Propane	0.40	8.0	3.2	3.31 ± 0.06
9.5% Methane	0.38	7.5	2.9	2.90 ± 0.14
18% Hydrogen	0.64	5.2	3.3	6.47 ± 0.16

Table 1 above gives a summary of flame speed parameters for the mixtures studied. It is important to note that all three mixtures have similar values of flame speed, which typically corresponds to the propagation speed of the flame observed in the laboratory frame. Despite having similar flame speeds however, lean hydrogen mixtures have a Lewis number less than unity and the increased thermal diffusion amplify hydrodynamic flame instabilities causing lean hydrogen mixtures to propagate faster. The final column of the table shows the average speed for the flame front to reach the thermocouple closest to ignition. While the data in this column shows that the propane and methane mixtures initially propagated at their laminar flame speeds it shows that hydrogen propagated almost twice as fast as its laminar flame speed. This result illustrates the need for a treatment of flame instabilities in modeling hydrogen deflagrations and provides a value to use in the development of the model.

The pressure-data presented in this section were all taken from readings of transducer P1 using an 80 Hz low pass filter. No significant differences were found in the readings between transducers. Flame velocities were calculated using flame time-of-arrival data from the line of thermocouples, with the positive direction toward the vent and negative direction toward the back wall.

Figures 4-6 below summarize the results of for different mixtures. The pressure time-histories seen in Fig. 4 show similar behavior between the propane and methane mixtures with the main difference that the propane peaks occur slightly earlier due to propane's higher laminar flame speed. While the hydrogen mixture has the same laminar flame speed as the propane mixture the pressure plots show much earlier pressure peaks and achieves significantly higher overall pressures than the propane or

methane mixtures. The reason for this can be seen in Fig. 5 where the flame velocity as a function of position is normalized by the theoretical laminar flame speed of the mixture. In this plot it can be seen that while methane and propane curves converge the hydrogen curve shows a significantly higher flame propagation speed.

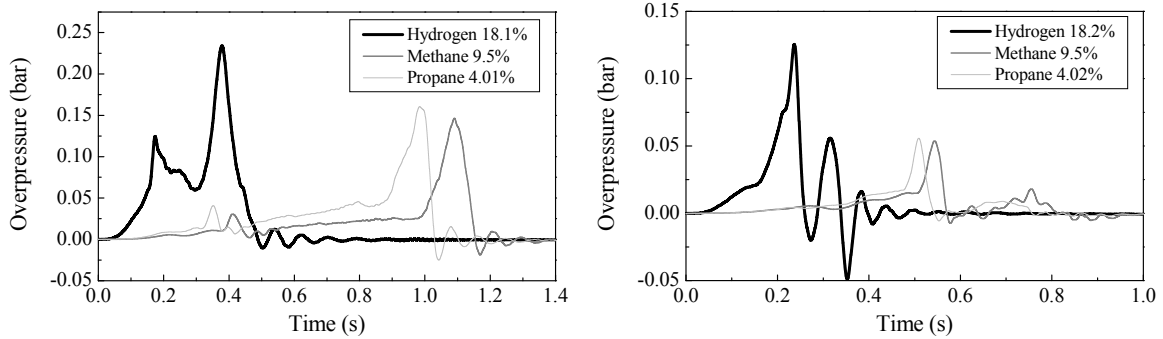


Figure 4. Pressure time history plots comparing hydrogen, methane and propane mixtures, center ignition 5.4 m^2 vent on the left, back-wall ignition, 2.7 m^2 vent on the right.

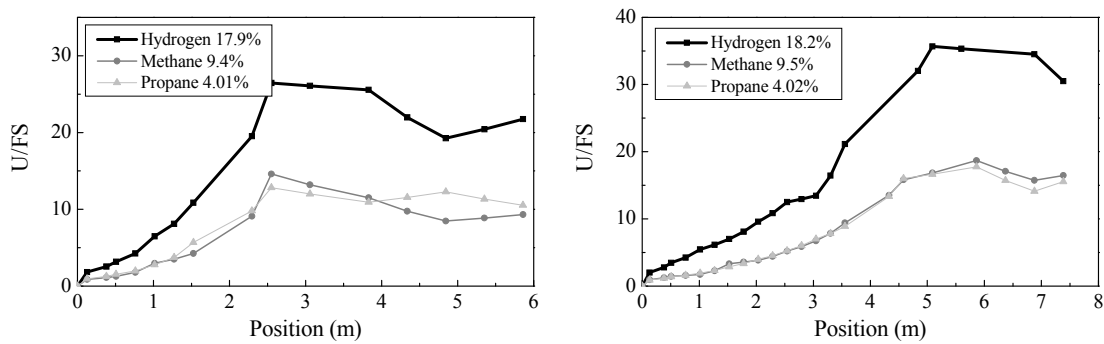


Figure 5. Velocity normalized by laminar flame speed for hydrogen, methane and propane mixtures, center ignition 5.4 m^2 vent on the left, back-wall ignition, 2.7 m^2 vent on the right.

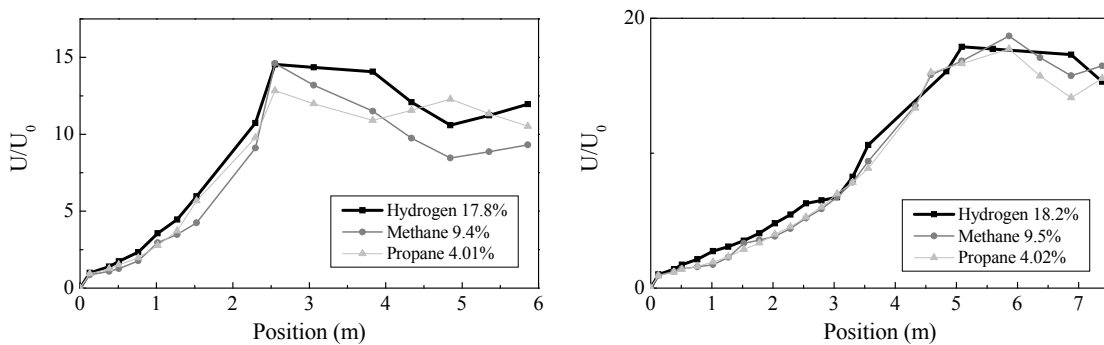


Figure 6. Velocity normalized by initial flame speed for hydrogen, methane and propane mixtures, center ignition 5.4 m^2 vent on the left, back-wall ignition, 2.7 m^2 vent on the right.

It is important to note however, that when the hydrogen velocity is normalized by its initial measured flame speed, shown in Fig. 6, the overall hydrogen velocity curve matches the methane and propane velocity curves. This implies that the enhancement of the hydrogen propagation speed caused by flame instabilities remains more or less constant throughout the combustion process.

4.3 Results of Hydrogen Tests:

Figure 7 shows the pressure-time history and flame velocity for an 18.2% hydrogen-air mixture with the 5.4 m² vent and back-wall ignition in the 64 m³ chamber. The test shows a large initial peak caused by the external explosion followed by a strong Helmholtz oscillation during which all the remaining combustion gas is consumed.

Figure 8 shows the pressure time-history and velocity for an 18.2% hydrogen-air mixture with the 5.4 m² vent and central ignition in the 64 m³ chamber. Compared to the back-wall ignition, the center ignition test shows a significantly lower maximum pressure as well as the formation of two distinct pressure peaks separated by a 0.15 s time where the pressure within the chamber drops to atmospheric.

The experiment with the 2.7 m² vent and back-wall ignition is shown in Fig. 9. In this test configuration a Helmholtz oscillation forms after the external explosion peak, as it does in the large vent back-wall ignition case, however the effect of the oscillation relative to the pressures within the chamber is much weaker than with the large vent.

The experiment with center ignition and the 2.7 m² vent is shown in Fig. 10. As with the large vent case the pressure-time history again shows two distinct peaks. However, in this case the second peak corresponds to a much higher pressure and the pressure between the peaks does not drop to atmospheric.

The effect of ignition location for both large and small vents can readily be seen in the results above. Back-wall and center ignition show greatly different behavior, with the maximum pressure for back-wall ignition corresponding to the external explosion which is then followed by a strong Helmholtz oscillation while center-ignition tests show two separate peaks: one caused by the external explosion and the other corresponding to the maximum flame surface area in the chamber. The increased effect of the external explosion in back-wall ignition tests is due to a larger cloud of unburned gas outside the chamber as well as higher propagation velocities as the flame exits the chamber. Consequently, the second peak observed in center-ignition cases does not appear in the back-wall ignition cases as the flame surface has already reached its maximum flame area at the time of the external explosion and more fuel is burned outside the chamber reducing the amount remaining in the chamber at the time of the external explosion.

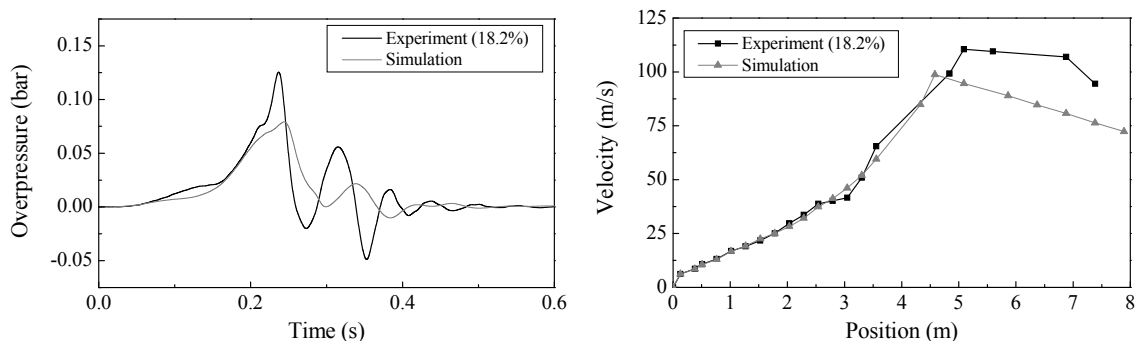


Figure 7. Pressure time history plots and velocity as a function of distance for lean hydrogen-air mixtures with a 5.4 m² vent and back-wall ignition.

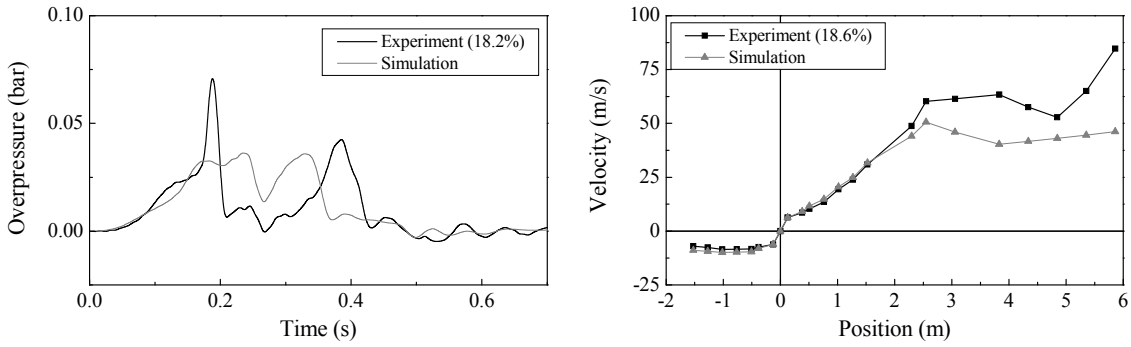


Figure 8. Pressure time history plots and velocity as a function of distance for lean hydrogen-air mixtures with 5.4 m² vent and central ignition.

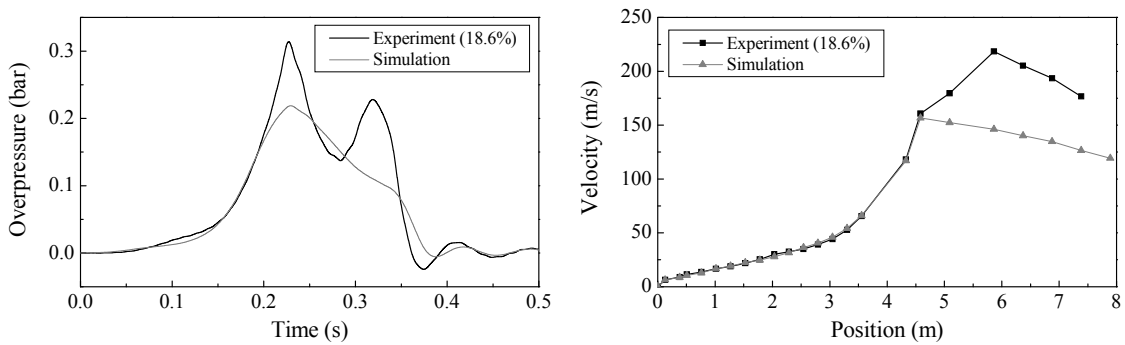


Figure 9. Pressure time history plots and velocity as a function of distance for lean hydrogen-air mixtures with a 2.7m² vent and back-wall ignition.

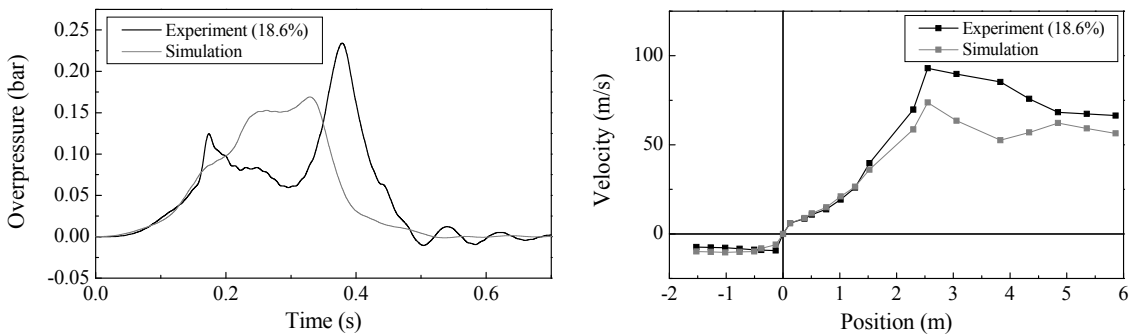


Figure 10. Pressure time history plots and velocity as a function of distance for lean hydrogen-air mixtures with a 2.7m² vent and central ignition.

4.4 Performance of CFD Model

The results of the simulations are shown in Figs. 7-10 in comparison with the test data. It is seen that the model gave good predictions for the flame speeds as a function of distance within the chamber. The difference is roughly of the order of the scatter seen between repeated tests. Initial pressure build-

up was also captured well by the model. The velocity profiles outside the chamber however, were significantly under predicted in all simulations.

For the back-wall ignition tests for both small vents as well as large vents the CFD model performs well, showing good agreement with the general shape while under predicting the maximum pressures observed. The small pressure peaks generated by the external explosion are not captured, which is consistent with the lower flame speeds observed outside of the chamber.

For the center ignition tests the CFD simulations fail to produce the two distinct pressure peaks seen in the experiments. Instead, the simulations produced a single larger peak. The maximum pressure was under predicted for both small and large vent center-ignition cases; however, neither result differed excessively from the experiments. It should be mentioned that the study with methane-air mixtures [16] did produce two peaks in cases with central ignition and had a closer appearance to experiments.

The primary difference seen between experiments and simulations with central ignition in lean hydrogen mixtures was that the first large pressure peak, caused by both the Helmholtz oscillation and the external explosion, was under predicted; and this was followed by the absence of a strong pressure drop. A possible cause for this difference is that the sequential “wrinkling” and “smoothing” of the flame surface due to the Taylor instability [16], caused by Helmholtz oscillations, were not resolved on the 5 cm mesh.

It should be noted that it is a physics-based model that was used in this study. For methane-air mixtures [16] it did not require the fitting of a set of constants to help mimic the explosion behavior. Only one constant was chosen in order to match the initial flame speed. With the lean hydrogen mixtures used in the present tests the situation was more complicated. The hydrodynamic instability enhanced by thermal diffusion effects results in a significant increase of the flame surface. The governing parameter for this instability, such as the cutoff scale, is not known for the mixture tested. The effect of the Lewis number on the turbulent burning velocity was another problem. The strength of this effect is currently not known well enough to be reliably modeled. These two unknowns gave certain flexibility in choosing the model parameters. This limitation emphasizes that more detailed data on basic properties of lean hydrogen flames are required for the development and validation of numerical models in general and the current model in particular.

5.0 CONCLUSIONS

Experiments were performed in FM Global’s 64 m³ chamber for 18% vol. hydrogen-air, 9.5% methane-air and 4.0 % propane-air mixtures for two ignition locations and two vent sizes. These experiments showed that despite having similar laminar flame speeds the hydrogen mixtures experimentally measured flame speed were much higher than the methane and propane mixtures due to flame instabilities. Due to the higher propagation speeds of the hydrogen flames significantly higher pressures were generated during the vented explosions when compared to the methane and propane mixtures.

Using the results of the hydrogen experiments, a numerical CFD model was tested and its capabilities and deficiencies were identified. It was found that the model gave a good prediction for the flame speeds as a function of distance within the chamber. Initial pressure build-up and flame propagation speeds were satisfactory captured the model, however flame speeds outside the chamber and maximum overpressures were under predicted. The primary difference seen between experiments was likely due to insufficient resolution of the external explosion, Taylor instability and Helmholtz oscillations, an area identified for further improvement of the model. It was also shown that there is a need for more detailed information on basic properties of lean hydrogen flames to be used for predictive explosion simulations. Further studies are necessary to explore improvements of the model and to validate the model over a wide representative range of test conditions.

ACKNOWLEDGEMENTS

The work presented in this paper was funded by FM Global and performed within the framework of the FM Global Strategic Research Program on Explosions and Material Reactivity. The authors are thankful to Franco Tamanini for many helpful discussions of the measurement techniques and test results. The technical assistance of Mike Gravel and Kevin Mullins in preparing and conducting the tests is greatly appreciated.

REFERENCES

1. Cooper, M.G., Fairweather, M. and Tite, J.P., On the Mechanisms of Pressure Generation in Vented Explosions, *Combustion and Flame*, **65**, 1986, pp. 1-14.
2. Zalosh, R.G., Gas Explosion Tests in Room-Size Vented Enclosures, Proceedings of the 13th Loss Prevention Symposium, 1979, Houston, pp. 98-108.
3. van Wingerden, C.J.M., On the Venting of Large-Scale Methane-Air Explosions, 6th International Symposium of Loss Prevention and Safety Promotion in the Process Industries, 19-22, June 1989, Oslo.
4. Bimson, S.J., Bull, D.C., Cresswell, T.M., Marks, P.R., Masters, A.P., Prothero, A., Puttock, J.S., Rowson, J.J. and Samuels, B., An Experimental Study of the Physics of Gaseous Deflagration in a Very Large Enclosure, Fourteenth International Colloquium on the Dynamics of Explosions and Reactive Systems, 1st – 6th, August 1993, Coimbra, Portugal.
5. Harrison, A.J. and Eyre, J.A., External Explosions as a Result of Explosion Venting, *Combustion Science and Technology*, **52**, 1987, pp. 91-106.
6. Solberg, D.M., Papas, J.A. and Skramstadt, E., Observations of Flame Instabilities in Large Scale Vented Gas Explosions, 18th Symp. (Int.) on Combustion, Waterloo, ON, The Combustion Inst., 1980, pp. 1607-1614.
7. Tamanini, F. and Chaffee, J.L., Combined Turbulence and Flame Instability Effects in Vented Explosions, Seventh International Symposium on Loss Prevention and Safety Promotion in the Process Industries, 1992, Taormina, pp. 38-11/38-19.
8. Tamanini, F., Characterization of Mixture Reactivity in Vented Explosions, Fourteenth International Colloquium on the Dynamics of Explosions and Reactive Systems, 1st – 6th, August 1993, Coimbra, Portugal.
9. Bradley, D. and Mitcheson, A., The Venting of Gaseous Explosions in Spherical Vessels, *Combustion and Flame* **32**, 1978, pp. 221-255.
10. Molkov, V.V., Innovative Vent Sizing Technology for Gaseous Deflagrations, Sixth International Symposium on Fire Safety Science, July, 1999, France, .
11. Molkov, V.V., Dobashi, R., Suzuki, M. and Hirano, T., Modeling of Vented Hydrogen-Air Deflagrations and Correlations for Vent Sizing, *Journal of Loss Prevention in the Process Industries*, **12**, 1999, pp. 147-156.
12. VDI 3673, Pressure Venting of Dust Explosions. Verein Deutscher Ingenieure, 1995.
13. NFPA 68, Standard on Explosion Protection by Deflagration Venting, 2007 Edition, National Fire Protection Association, Quincy, MA 02269, 2007.
14. Watterson, J.K., Connel, I.J., Savill, A.M. and Dawes, W.N., A Solution Adaptive Mesh Procedure for Predicting Confined Explosions, *International Journal for Numerical Methods in Fluids*, **26**, 1998, pp. 235–247.
15. Molkov, V., Makarov, D. and Puttock, J., The Nature and Large Eddy Simulation of Coherent Deflagrations in a Vented Enclosure-Atmosphere System, *Journal of Loss Prevention in the Process Industries*, **19**, 2006, pp. 121-129.

16. Bauwens, C.R., Chaffee, J. and Dorofeev, S., Experimental and Numerical Study of Methane-air Deflagrations in a Vented Enclosure, Sixth International Symposium on Fire Safety Science, September, 2008, Germany.
17. Weller, H.G. and Tabor, G., A Tensorial Approach to Computational Continuum Mechanics Using Object-Oriented Techniques, *Computers in Physics*, **12**, No. 6, 1998, pp. 620-631.
18. Issa, R. I., Solution of the Implicitly Discretised Fluid Flow Equations by Operator-Splitting, *Journal of Computational Physics*, **62**, 1986, pp. 40-65.
19. Fureby, C., Tabor, G., Weller, H.G. and Gosman, A.D., A Comparative Study of Subgrid Scale Models in Homogeneous Isotropic Turbulence, *Physics of Fluids*, **9**, No 5, 1997, pp. 1416-1429.
20. Weller, H. G., Tabor, G., Gosman, A.D. and Fureby, C., Application of a Flame-Wrinkling LES Combustion Model to a Turbulent Mixing Layer, 27th Symp. (Int.) on Combustion, Boulder, CO, The Combustion Inst., 1998, pp. 899-907.
21. Bychkov V., Importance of the Darrieus-Landau Instability for Strongly Corrugated Turbulent Flames, *Physical Review E*, **68**, 2003.
22. Bradley, D., Sheppard, C.G.W., Woolley, R., Greenhalgh, D.A. and Lockett, R.D., The Development and Structure of Flame Instabilities and Cellularity at Low Markstein Numbers in Explosions, *Combustion and Flame*, **122**, 2000, pp. 195–209.
23. Bradley, D., Lawes, M., Liu, K., Verhelst, S. and Woolley, R., Laminar Burning Velocities of Lean Hydrogen–Air Mixtures at Pressures Up To 1.0 MPa, *Combustion and Flame*, **149**, 2007, pp. 162–172.
24. Bradley, D., Lau, A.K.C. and Lawes, M., Flame Stretch Rate as a Determinant of Turbulent Burning Velocity, *Philosophical Transactions of the Royal Society of London, Series A*, **338**, 1992, pp. 359-387.
25. Driscoll, J.F., Turbulent Premixed Combustion: Flamelet Structure and Its Effect on Turbulent Burning Velocities, *Progress in Energy and Combustion Science*, **34**, 2008, pp. 91-134.